Published in final edited form as:

Nat Genet. 2017 October ; 49(10): 1529–1538. doi:10.1038/ng.3933.

Mutations in the evolutionarily highly conserved KEOPS complex genes cause nephrotic syndrome with microcephaly

A full list of authors and affiliations appears at the end of the article.

Abstract

Galloway-Mowat syndrome (GAMOS) is a severe autosomal-recessive disease characterized by the combination of early-onset steroid-resistant nephrotic syndrome (SRNS) and microcephaly with brain anomalies. To date, mutations of *WDR73* are the only known monogenic cause of GAMOS and in most affected individuals the molecular diagnosis remains elusive. We here identify recessive mutations of *OSGEP*, *TP53RK*, *TPRKB*, or *LAGE3*, encoding the 4 subunits of the KEOPS complex in 33 individuals of 30 families with GAMOS. CRISPR/Cas9 knockout in

Correspondence should be addressed to: Martin Zenker, M.D., Institute of Human Genetics, University Hospital Magdeburg, Leipziger Str. 44, 39120 Magdeburg, Germany, Phone: +49 391 67 15064, martin.zenker@med.ovgu.de or Corinne Antignac, M.D., Ph.D., INSERM U1163, Institut Imagine, 24, bd du Montparnasse, 75015 Paris, France, Phone: +33 1 42 75 43 45, corinne.antignac@inserm.fr or Friedhelm Hildebrandt, M.D., Boston Children's Hospital, Enders 561, Harvard Medical School, 300 Longwood Avenue, Boston, MA 02115, USA, Phone: +1 617-355 6129, Fax: +1 617-730 0569, friedhelm.hildebrandt@childrens.harvard.edu.
*These authors contributed equally to this work.

ACCESSION NUMBERS

LAGE3 (NM_006014.4), *OSGEP* (NM_017807.3), *TP53RK* (NM_033550.3), *TPRKB* (NM_016058.2).

Competing interests statement

M.T.C., A.B., and R.E.S. are employees of GeneDx, Gaithersburg, MD, USA.
The other authors declare that they have no competing financial interests.

AUTHOR CONTRIBUTIONS

1. J.R., G.M., D.S., W.T., O.G., S.A., De.S., N.B., Ga.M., S.L., M.F., B.M., S.V., N.dR., M.A., T.H., S.S., E.W., H.Y.G., W.I.C., C.E.S., W.L.P., J.W., A.D., W.M., A.B., R.E.S., S.M., R.P.L., M.Z., C.A. and F.H. generated total genome linkage data, performed exome capture with massively parallel sequencing, and performed whole exome evaluation and mutation analysis.
2. D.A.B. generated knockdown cell lines, performed *in-vitro* studies (proliferation, survival, apoptosis, and migration) in immortalized human podocytes, and performed co-immunoprecipitation experiments.
3. D.A.B. and J.A.L. performed immunofluorescence and subcellular localization studies in tissue sections and cell lines by confocal microscopy.
4. J.R., W.T., J.W., D.A.B., O.B., Ba.B., Br.B., Ma.B., G.S.C.,J.H.C., M.T.C., P.G., C.K.B., Y.Y.K., W.M.L., E.L., S.P.L., R.O.L., A.M., M.M., K.N., M.P., A.P., C.P., P.R., T.S., M.S., N.A.S., K.S., W.H.T., J.D.T., Da.S., M.H.T., U.V., D.H.V., N.V., J.L.W., M.T.F.W., S.N.W., P.K., D.C., D.M., B.C., M.Z., C.A., and F.H. recruited patients and gathered detailed clinical information for the study.
5. M.C.D., Br.C., D.L., T.B.L., and H.V.T. performed yeast complementation experiments, and 3D modeling of the KEOPS complex.
6. I.C.G. and G.M. performed proteomic studies in human podocyte cell lines
7. P.R. performed telomere restriction fragment assay
8. T.J.S., J.M.S., A.P., and G.T. performed zebrafish experiments and data analysis.
9. O.S.F. and M.B. performed CRISPR/Cas9 knockout in mouse embryos and subsequent embryonic phenotyping.
10. All authors critically reviewed the paper.
11. M.Z., C.A. and F.H. conceived of and directed the project and wrote the paper, with the help of D.A.B., G.M. and H.V.T.

zebrafish and mice recapitulates the human phenotype of microcephaly and results in early lethality. Knockdown of *OSGEP*, *TP53RK*, or *TPRKB* inhibits cell proliferation, which human mutations fail to rescue, and knockdown of either gene activates DNA damage response signaling and induces apoptosis. OSGEP and TP53RK molecularly interact and co-localize with the actin-regulating ARP2/3 complex. Furthermore, knockdown of *OSGEP* and *TP53RK* induces defects of the actin cytoskeleton and reduces migration rate of human podocytes, an established intermediate phenotype of SRNS. We thus identify 4 novel monogenic causes of GAMOS, describe the first link between KEOPS function and human disease, and delineate potential pathogenic mechanisms.

RESULTS

Mutations of KEOPS complex encoding genes in patients with Galloway-Mowat syndrome

Galloway-Mowat syndrome (GAMOS, MIM #251300), a distinct renal-neurological disease, is characterized by early-onset nephrotic syndrome (NS) associated with microcephaly, brain anomalies, and developmental delay.[1–3] Seeking additional monogenic causes of NS we performed homozygosity mapping[4] and whole exome sequencing (WES)[5] in 91 families. In consanguineous family B57 (Supplementary Fig. 1A) with GAMOS we detected a homozygous missense mutation (p.Ile14Phe) in the gene *OSGEP* (Supplementary Table 1, Fig. 1, Supplementary Fig. 1–2). *OSGEP* encodes the tRNA N6-adenosine threonylcarbamoyltransferase protein OSGEP, a unit of the highly conserved KEOPS complex (Kinase, Endopeptidase and Other Proteins of small Size). The KEOPS complex contains 4 subunits LAGE3, OSGEP, TP53RK, and TPRKB. It regulates a universal chemical modification of tRNAs that is necessary for translational accuracy and efficiency.[6–9] Other known functions relate to control of telomere length, genome maintenance,[10,11] and regulation of gene transcription.[12] Furthermore, the KEOPS complex has been implicated in telomere associated DNA damage response (DDR) signaling, and exhibits intrinsic DNA binding ability.[13,14]

Using WES and high-throughput exon sequencing,[15,16] we then screened the coding regions of *OSGEP*, *TP53RK*, *TPRKB* and *LAGE3* in 907 individuals with NS including 91 individuals with GAMOS. We discovered mutations in all 4 genes in 33 individuals with GAMOS from 30 different families (Supplementary Table 1, Supplementary Fig. 1–3). We did not detect mutations in families with isolated NS. Specifically, we discovered recessive *OSGEP* mutations in 22 families (15 different alleles), *TP53RK* mutations in 3 families (4 different alleles), *TPRKB* mutations in 2 families (2 different alleles), and *LAGE3* mutations in 3 families (3 different alleles) (Fig. 1, Supplementary Fig. 1–3, Supplementary Table 1). Inheritance was autosomal recessive or X-linked (*LAGE3*). Multiple *OSGEP* mutations were shared between different families from distinct ethnicities, most likely representing geographic founder alleles from Iran, Taiwan, and Europe (Supplementary Table 1).

Clinical features in KEOPS complex mutations

Phenotypically, all individuals with mutations in any of the 4 KEOPS genes had primary microcephaly, developmental delay, propensity for seizures, and NS of early onset (Fig. 1, Supplementary Fig. 4, Table 1, Supplementary Table 1). Most patients died in early childhood. Several individuals were noted to have facial dysmorphism sometimes with

features of progeria, and skeletal abnormalities such as arachnodactyly. The most frequently observed brain anomalies included a spectrum of gyration abnormalities ranging from lissencephaly to pachygyria and polymicrogyria, and cerebellar hypoplasia (Fig. 1, Supplementary Fig. 4, Table 1, Supplementary Table 1).

Renal biopsy revealed focal-segmental glomerulosclerosis (FSGS), its developmental equivalent, diffuse mesangial sclerosis (DMS),[17] or other glomerular lesions in 16 individuals in whom a renal biopsy was performed. Electron microscopy revealed partial podocyte foot process effacement (Fig. 1, Supplementary Fig. 4, Table 1, Supplementary Table 1). Because of the early onset of nephrotic syndrome, only in 3 individuals a therapeutic attempt was made with corticoids or cyclosporin A. However, none of these individuals responded to any treatment regimen as expected in FSGS or DMS.[18]

We thereby discovered recessive mutations in any of the 4 genes encoding KEOPS complex proteins as novel causes of Galloway-Mowat syndrome. We termed these variants of GAMOS due to mutations in *LAGE3*, *OSGEP*, *TP53RK*, or *TPRKB*, 'GAMOS 2', 'GAMOS 3', 'GAMOS 4' and 'GAMOS 5', respectively. Thus, we made the surprising discovery, that specific recessive mutations in 4 genes that serve a fundamental cellular function cause a distinct renal-neuronal disease phenotype. It is important to note that none of the affected individuals with autosomal recessive mutations carried two truncating alleles in the mutated gene (Supplementary Table 1).

Brain phenotype in zebrafish and mouse models

To evaluate the pathogenic effects of KEOPS protein loss of function in an *in vivo* animal model we performed CRISPR/Cas9 knockout of the orthologous zebrafish genes *osgep*, and *tprkb*. Knockout of *osgep* (Supplementary Fig. 5) or *tprkb* (Supplementary Fig. 6) in zebrafish larvae recapitulated a microcephaly phenotype as encountered in humans with KEOPS gene mutations. Head size reduction was not secondary to growth retardation, since the body length was not reduced compared to the control groups for neither gene (Supplementary Fig. 5–6). Because most patients with *OSGEP* mutations died in early childhood, we generated Kaplan-Meyer-survival curves for zebrafish with CRISPR/Cas9 knockout of *osgep* or *tprkb* and found that knockout fish show early lethality (Supplementary Fig. 7). In particular, all homozygous larvae died within 15 or 18 days post fertilization for *osgep* and *tprkb,* respectively.

We then examined an embryonic mouse model for recapitulation of human GAMOS phenotypes. Mouse embryos with CRISPR/Cas9 knockout of *Lage3, Osgep,* or *Tprkb* had significantly reduced cortex length, cortex – midbrain midline length, and cortex width, and thus reproduced the human microcephaly phenotype (Supplementary Fig. 8).

We did not observe a renal phenotype in knockout mice or fish. We hypothesize that this is due to early lethality masking renal involvement that might occur in older animals.

Functional and structural assessment of the mutations in the KEOPS complex

Using the available crystal structures of homologous subassemblies of the KEOPS complex, [19–21] we constructed a 3D model of the human complex. The subunits are arranged in a

linear fashion in the order LAGE3-OSGEP-TP53RK-TPRKB (Fig. 2a). OSGEP constitutes the catalytic subunit of the complex while the other subunits are obligatory for t6A modification, but their biochemical contribution is not understood.[19,20] Projection of the various mutations onto the 3D model of KEOPS and incorporation of the sparse mechanistic knowledge of the complex (Fig. 2a),[7,8,19,20] led us to classify the mutations into three classes according to their putative biochemical effects: (1) those that might perturb folding and/or protein interaction (*LAGE3*: Val106Phe; *OSGEP*: Val107Met, Lys198Arg, Arg247Gln, Arg280His; *TP53RK*: Thr81Arg; *TPRKB*: Leu136Pro, Tyr149Cys) (2) those that might perturb interaction with the tRNA substrate (*OSGEP:* Arg325Trp/Gln; *TP53RK:* Arg243Leu), and (3) those in residues near the essential histidines in the active site of OSGEP (Ile14Phe, Cys110Arg, Ile111Thr) that may weaken catalytic activity. Using a yeast-based functional growth complementation assay (Fig. 2b) two functional classes of *OSGEP* mutant alleles were identified: Hypomorphic alleles that restore growth but to a lesser extent than the wild-type OSGEP, and amorphic alleles that completely fail to restore growth. Mutations corresponding to hypomorphic alleles (Lys198Arg, Arg247Gln, Arg280Cys and Arg325Gln) are localized mostly in regions involved in interactions with the Pcc1 (*Lage3*) and Bud32 (*TP53RK*) subunits, leading to a mild phenotype. Conversely, mutations corresponding to amorphic alleles (Ile14Phe, Ile111Thr and Cys110Arg) are in close vicinity to the catalytic cleft residues, resulting in a severe phenotype.

Furthermore, we show by co-immunoprecipitation experiments that the truncating mutation p.Lys60Serfs*61 and the missense mutation p.Thr81Arg of *TP53RK* detected in the siblings of family B77 both abrogated the interaction between TPRKB and TP53RK (Fig. 2c). Other mutations of any of the 4 genes did not abrogate intermolecular interactions (Supplementary Fig. 9–11).

Role of KEOPS proteins in cell proliferation and DDR

We first evaluated subcellular localization of all 4 KEOPS proteins, either endogenous or overexpressed as Myc- or GFP-tagged proteins. We found that all 4 proteins localize both to the cytoplasm and the nucleus in podocyte cell lines (Supplementary Fig. 12–13). Furthermore, we demonstrated by mass spectrometry in a human podocyte cell line stably over-expressing LAGE3 as well as by coimmunoprecipitation in HEK cells that all three subunits co-purified with LAGE3 indicating that a complete KEOPS complex is formed in human cell lines (Supplementary Fig. 14).

Genetic deletion of KEOPS genes results in severe growth defects in yeast.[12] We therefore tested whether knockdown of *OSGEP, TP53RK*, or *TPRKB* also altered proliferation of mammalian cells and found that stable knockdown of these genes in human podocytes impaired cell proliferation rate using a BrdU assay (Fig. 2d) and the XCELLigence® system (Supplementary Fig. 15A). The proliferation defect was rescued by reexpressing wildtype but not mutant proteins of the respective mouse cDNAs (Fig. 2e–f; Supplementary Fig. 15B) showing that the identified human disease alleles impair protein functionality.

We observed that after 4–5 passages human podocyte cell lines with stable knockdown of *OSGEP, TP53RK,* or *TPRKB* exhibited severely reduced cell survival and increased apoptosis as demonstrated by elevated caspase-3 activity (Fig. 3a). Because the KEOPS

complex has been implicated in genome maintenance,[13,14] we tested whether the observed induction of apoptosis could be elicited by activation of DNA damage response signaling (DDR). We found that stable knockdown of *OSGEP, TP53RK*, or *TPRKB* in human podocyte cell lines increased immunofluorescence staining for γH2AX, indicating DDR activation (Fig. 3b, Fig. Supplementary Fig. 16A). We confirmed increased γH2AX by immunoblotting in knockdown podocyte cell lines (Fig. 3c–d, Supplementary Fig. 17) and in fibroblasts from patients with GAMOS and mutations of *OSGEP* or *TPRKB* (Supplementary Fig. 16B).

DDR activation results in cell cycle arrest in order to allow DNA repair, if possible. Alternatively, if DNA damage is too severe, induction of apoptosis avoids propagation of cells with damaged genetic material. In order to elucidate the sequence of DDR activation and induction of apoptosis, we performed immunoblotting of γH2AX, and caspase-3 at 3 different time points after stable knockdown of *OSGEP* in human podocyte cell lines (Fig. 3c–d). We found increased protein levels of γH2AX and the CDK inhibitor p21 on days 5, 7, and 9 after knockdown. Conversely, the proapoptotic factor BAX and cleaved Caspase-3 only showed strong induction on days 7 and 9 (Fig. 3c–d). The time course suggested that, as expected, γH2AX activation precedes induction of apoptosis. Induction of γH2AX, p21, BAX, and caspase-3 were also found in podocytes with stable knockdown of *TP53RK* or *TPRKB* (Supplementary Fig. 17). We further confirmed genomic instability in KEOPS knockdown cells by showing that the genotoxic agent mitomycin-C induced apoptosis in *OSGEP, TP53RK,* or *TPRKB* knockdown cell lines at concentration that did not affect control cells (Supplementary Fig. 18). To further elucidate the role of KEOPS proteins in DDR, we characterized an antibody against TP53RK in rat kidney sections (Supplementary Fig. 19–20) and found that TP53RK colocalizes with the DNA repair protein PARP1 in renal glomeruli (Figure 3e). Similarly, we found colocalization of OSGEP and PARP1 in human podocyte cell lines (Supplementary Fig. 20C). Co-immunoprecipitation experiments in HEK293T cells demonstrated that all four members of the KEOPS complex precipitate endogenous PARP1 (Figure 3f) suggesting a potential link between KEOPS and PARP1 function that might contribute to the induction of DDR seen upon knockdown of KEOPS genes.

Microcephaly is a feature common to various syndromes of defective DDR[22–25] likely due increased apoptosis of neuronal progenitor cells. Furthermore podocyte loss has been described as an important pathomechanism of renal glomerulosclerosis.[26] We therefore propose that induction of DDR and increased apoptosis are likely an integral part of the pathogenesis of GAMOS in individuals with mutations in KEOPS genes.

Although it has been shown in yeast that mutants of KEOPS subunits exhibit shortened telomeres[27] and some patients with microcephaly have shortened telomeres,[28] telomere length of affected children was in the normal range for their age and in comparison with their parents, suggesting that the KEOPS complex mutations do not affect telomere maintenance (Supplementary Fig. 21).

Regulation of podocyte actin cytoskeleton organization by the KEOPS complex

Upon EGF stimulation, OSGEP and TP53RK were suggested to interact with proteins of the ARP2/3 complex,[29] which are essential regulators of actin remodeling at lamellipodia.[30] In this context it is of interest that lamellipodia formation and actin remodeling are considered important cellular functions of podocytes and are impaired in monogenic forms of SRNS.[31] We thus first confirmed by coimmunoprecipitation in HEK293T cells that OSGEP and TP53RK interacted with 4 ARP complex proteins, namely ARPC1B, ARPC2, ACTR2, and ACTR3 (Fig. 4a–c and Supplementary Fig. 22).

We then found that upon EGF stimulation, which induces formation of the sub-lamellipodia actin network, OSGEP and TP53RK colocalized with ARP2 and ARP3 at lamellipodia in human podocytes (Fig. 4d). Interestingly, in *OSGEP* and *TP53RK* knockdown podocyte cell lines the formation of the sub-lamellipodia actin network was severely disrupted (Fig. 4e), a finding that is likely relevant for the SRNS pathogenesis.

We then studied podocyte migration, a well-established surrogate phenotype of SRNS, that is typically altered upon loss-of-function of genes that if mutated cause monogenic forms of SRNS.[32–34] We found that podocyte migration, assessed in a scratch wound assay, was reduced in podocytes with knockdown of *OSGEP*, *TP53RK*, and *TPRKB* (Fig. 4f). We conclude that the KEOPS proteins OSGEP and TP53RK play a role in actin regulation, lamellipodia formation, and cell migration, and that these mechanisms likely contribute to the pathogenesis nephrotic syndrome upon alterations of KEOPS proteins.

In conclusion, we have demonstrated that specific mutations in genes encoding the four subunits of the KEOPS complex are newly identified monogenic causes of GAMOS. We delineate impaired cell proliferation, increased apoptosis, genomic instability, and defects in actin regulation as possible pathogenic features.

ONLINE METHODS

Study participants

We obtained blood samples and pedigrees following informed consent from individuals with NS / GAMOS or their legal guardians. Approval for human subjects research was obtained from Institutional Review Boards of the University of Michigan, Boston Children's Hospital, the University of Erlangen, and the Comité de Protection des Personnes Ile de France II.

Homozygosity mapping and whole exome sequencing

Whole exome sequencing was performed as described previously[1] using Agilent SureSelect™ human exome capture arrays (Thermo Fisher Scientific) with next generation sequencing (NGS) on an Illumina™ platform. Sequence reads were mapped against the human reference genome (NCBI build 37/hg19) using CLC Genomics Workbench (version 6.5.1) (CLC bio). For homozygosity mapping, downstream processing of aligned BAM files were done using Picard and samtools.[2] SNV calling was done using GATK5 and the generated VCF file was subsequently used in homozygosity mapper.[3] Genetic regions of

homozygosity by descent were plotted across the genome as candidate regions for recessive genes as previously described.[4] Mutation calling was performed in line with proposed guidelines[5] by scientists, who had knowledge of clinical phenotypes, pedigree structure, and genetic mapping.

High-throughput mutation analysis by array-based multiplex PCR and NGS

We utilized the 48.48 Access Array microfluidic technology (Fluidigm™) to perform barcoded multiplex PCR as described previously.[6,7] A total of 91 individuals with NS and brain anomalies as well as 816 individuals with isolated NS were sequenced. 2 x 250bp paired-end sequencing was performed on an Illumina™ MiSeq instrument. Sequence alignment was conducted using CLC Genomics Workbench (CLC bio). Mutations were confirmed by Sanger sequencing and evaluated for segregation.

Generation and phenotypic characterization of stable zebrafish knockout lines by CRISPR/Cas9

Target selection and sgRNA generation—Single guide RNA (sgRNA) targets were selected using the CHOPCHOP online tool (https://chopchop.rc.fas.harvard.edu[8]) following their ranking algorithm. The algorithm takes in to account all potential off-targets differing in up to 2 nucleotides, GC-content and presence of a guanine residue in the last position before the Protospacer Adjacent Motif (PAM) sequence since these factors influence the efficiency of sgRNA binding and Cas 9 cleavage.[9] Targets were chosen in the early exons to potentially introduce early frameshift mutations to maximize loss of function of the protein. gRNAs were generated by *in-vitro* transcription from oligonucleotide based templates using the MEGAscript T7 Transcription kit (Ambion) as described before.[9] Since gRNA activity is higher if 2 Guanine bases follow the T7 promotor, template sequences were modified accordingly if necessary. The resulting change of one or two nucleotides in the 5' end of the gRNA results in a higher indel frequency[9] and does not reduce specificity.[10]

Microinjection, mutation analysis and breeding—2 μl of sgRNA stock (500 ng/μl) were mixed with 2 μl of recombinant Cas 9 protein (1 μg/μl, PNA Bio, Thousand Oaks, CA) and incubated on ice for at least 10 min to allow formation of the sgRNA/Cas9 complex. 2 nl of the injection mix was injected intracellular in one cell stage zebrafish embryos using glass needles and a micromanipulator. DNA was extracted from 10 pooled injected embryos and an uninjected control group at 48 hours post fertilization using the HotShot protocol.[11] Mutagenesis was determined by a T7 endonuclease assay as described before.[12] Positive clutches (F0 generation) were raised to adulthood and outcrossed against wildtype fish. Germline transmission was also determined by the T7 endonuclease assay. Positive clutches (F1 generation) were raised to adulthood and genotyped individually. Fish carrying the same mutation were pooled being the founders of the heterozygous stable knock out line.

Microcephaly assay in Zebrafish—Zebrafish larvae at 4 days post fertilization (dpf) were embedded in 1% ultra-low gelling temperature agarose (Type IX-A, Sigma-Aldrich, St. Louis, MO) and imaged under a microscope (Zeiss, Germany) from a dorsal view. Total body length and head diameter through the rear third of the eye lens were measured using ImageJ, the measuring person being blinded for the genotype. Head diameter to total body

length ratio was calculated as an index for microcephaly. Significant differences were calculated using the one-way ANOVA test with multiple comparisons and a standard confidence interval of 95%.

Generation and phenotypic characterization of transient KEOPS mutant mouse embryos by CRISPR/Cas9

The murine genomic regions equivalent to the human mutations in *LAGE3* (Phe137Ser), *OSGEP* (Ile14Phe), *TP53RK* (Arg243Leu) and *TPRKB* (Leu136Pro) genes were analyzed for CRISPR/Cas9 target sites using the software package Spacer Scoring for CRISPR (SSC) (http://crispr.dfci.harvard.edu/SSC), and "Optimized CRISPR Design" tool (http://crispr.mit.edu/). Four different sgRNAs, each one targeting a different KEOPS gene were selected based on efficiency score and low off-target effect. sgRNA were synthesized *in vitro* following standard procedures and Cas9 mRNA was purchased from Sigma (Cas9mRNA-1EA). A mix of sgRNA (100 ng/μL) and Cas9mRNA (100 ng/μL) for each gene or a scramble sg RNA for Ctl embryos (WT) was co-injected into the cytoplasm of fertilized eggs and transferred into pseudopregnant females. Transient CRISPR/Cas9 E18.5 embryos were recovered and analyzed for microcephaly phenotypes. The occurrence of gene editing was confirmed by PCR amplification from extracted genomic DNA, followed by Sanger sequencing. Targeting efficiency was quantified by the Tracking of Indels by Decomposition (TIDE) web tool. Brain morphology and microcephaly phenotype was assessed by measuring cortex length, cortex midbrain midline length, and cortex width for WT and targeted CRISPR embryos. Statistical analysis was performed by using GraphPad Prism software version 6.0. An unpaired Student t-test was used to test for differences between the means.

3D modeling

3D models of the human KEOPS complex were obtained using the Phyre server (http://www.sbg.bio.ic.ac.uk/phyre2/html/).[13] The highest confidence models were retrieved for the LAGE3, OSGEP and TP53RK components. The structure of the human TPRKB protein was available at the PDB (code 3ENP). The model of the human KEOPS was constructed by superposing the structures of the human subunits onto the archaeal Pcc1/Kae1 (PDB code 3ENO) and Kae1/Bud32 (PDB code 3VWB) and the fungal Bud32/Cgi121 (PDB code 4WW9) subcomplexes. The sequences and structures of the interfaces between the subunits are well conserved. The LAGE3 Phe137Ser and TP53RK Gly42Asp mutations fell out of sequence regions that could be confidently modeled and are therefore not represented on Figure 2a.

Heterologous complementation assay of yeast Δ*kae1* mutant

The haploid conditional yeast *kae1* mutant strain (DL344) was derived from W303 genetic background and contains a genomic deletion of *KAE1* gene complemented by an *URA3*-plasmid borne *KAE1* wild type allele (kindly provided by Domenico Libri, Institut Jacques Monod, Paris, France). Human cDNAs encoding wildtype or mutant OSGEP were cloned in the yeast multicopy vector pESC-*TRP1* (Agilent technologies) under the control of the yeast strong inducible promoter P_{GAL10}. Native pESC-*TRP1* plasmid and a pFL39 plasmid carrying the yeast wild-type *KAE1* gene were used as negative and positive controls,

respectively. The various plasmids were introduced in the *kae1* mutant strain. After selection on glucose-Trp solid medium, transformant clones were streaked onto Gal-Trp + 5FOA medium to chase out the *URA3-KAE1* plasmid. Serial dilutions of cell suspensions prepared from colonies growing of 5FOA plates were spotted on Gal-Trp medium and incubated at 28°C to monitor growth complementation. Expression of human OSGEP constructs was confirmed by western blot using an anti-OSGEP antibody (HPA039751, Sigma Life Science) (Supplementary Fig. 23)

Proteomic studies

A human podocyte cell line stably expressing the human LAGE3 subunit fused to N-terminal V5 epitope was used to perform proteomic studies. Co-immunoprecipitation was performed using μMACS Protein A Microbeads Isolation Kit (Miltenyi Biotec) for the isolation of V5- tagged LAGE3. Briefly, podocytes cell lysates containing 1.5 mg of protein were incubated with 2 μg of mouse anti-V5 antibodies (Bio-Rad, MCA1360) for one hour at 4°C followed by 30 minutes incubation with 50 μl of Protein A Microbeads and finally applied onto μMACS Separation Columns (Miltenyi Biotec). Protein isolation was further performed according to the manufacturer's recommendations. The immunoprecipitation eluates were processed by FASP as described in Lipecka et al. (2016).[14] Peptides were dried in a Speedvac and resuspended in 10% acetonitrile (ACN), 0.1% TFA prior nanoRSLC-Q exactive Orbitrap Plus MS analysis (Dionex RSLC Ultimate 3000, *Thermo Fisher Scientific*). Raw files were analyzed using MaxQuant 1.5.5.1 software[15] against the Human Uniprot KB/Swiss-Prot database 2016-01. The false discovery rates (FDRs) at the protein and peptide level were set to 1%. Scores were calculated in MaxQuant as described previously.[15] Statistical and bioinformatic analysis, including volcano plot, were performed with Perseus software version 1.5.5.3 (freely available at www.perseus-framework.org).[16] For statistical comparison, two groups were set up, each containing 3 biological replicates: control IP and IP LAGE3. Only proteins that were quantified at least 3 times out of 6 were retained. T-test was performed and the data were represented on a volcano plot (FDR<0.01, S0=2, 250 randomizations) (Supplementary Fig. 14).

cDNA cloning

Human LAGE3, OSGEP, TP53RK, and TPRKB full-length cDNA were subcloned by PCR from human full-length cDNA (NM_006014.4, NM_017807.3, NM_033550.3, NM_016058.2). Mouse Osgep, Tp53rk, Tprkb were subcloned by PCR from human full-length cDNA (NM_133676.2, NM_023815.4, NM_001170488.1). Human ARPC1B, ARPC2, ACTR2, and ACTR3 were subcloned by PCR from human full-length cDNA (NM_005720.3, NM_005731.3, NM_001005386.2, NM_005721.4). cDNA was subcloned into the pENTR-D-TOPO vector (Thermo Fisher). Subsequently, expression vectors were generated using LR clonase (Thermo Fisher) following the manufacturer's instruction. The following expression vectors were used in this publication: pRK5-N-Myc, pCDNA6.2-N-GFP (Thermo Fisher), pDEST69-N-FLAG, pLenti-V5-DEST™ (Thermo Fisher), and pSirenRetroQ (Clontech). Clones reflecting the mutations identified in individuals with SRNS were introduced in the cDNA constructed using the Quick change II XL site-directed mutagenesis kit (Agilent Technologies) following the manufacturer's instructions. cDNAs were subcloned into the pENTR-D-TOPO or pDONOR221 vector (Thermo Fisher).

Subsequently, expression vectors were generated using LR clonase (Thermo Fisher) following the manufacturer's instruction. The following expression vectors were used in this publication: pRK5-N-Myc, pCDNA6.2-N-GFP (Thermo Fisher), pDEST69-N-FLAG, pLenti-V5-DEST™ (Thermo Fisher), and pSirenRetroQ (Clontech). Clones reflecting the mutations identified in individuals with GAMOS were introduced in the cDNA constructed using the Quick change II XL site-directed mutagenesis kit (Agilent Technologies) following the manufacturer's instructions.

Primary Antibodies (Validation: Supplementary Fig. 24–25)

Target protein	Company	Catalogue #	Species	Dilution (IF)	Dilution (WB)
LAGE3	LS Bioscience	LS-C201798	Rabbit	1:200	1:1,000
OSGEP	Novus biologicals	NBP2-00823	Mouse	1:400	1:1,000
TP53RK	Abgent	AP17010b-ev	Rabbit	1:200	1:1,000
TP53RK	Santa Cruz Biotechnology	sc-85846	Goat	1:100	1:1,000
TPRKB	Abcam	ab128112	Mouse	1:200	n/a
TPRKB	Abcam	ab96261	Rabbit	n/a	1:1,000
ARP2	Abcam	ab128934	Rabbit	1:200	1;1,000
Phospho-Histone H2A.X	Cell Signaling	(#9718)	Rabbit	1:200	1;1,000
Histone H2A.X	Cell Signaling	(#2595)	Rabbit	n/a	1;1,000
PARP1	Sigma Aldrich	HPA045168	Rabbit	1:200	1;1,000
p21 Waf1/Cip1	Cell Signaling	(#2947)	Rabbit	n/a	1;1,000
BAX	Cell Signaling	(#5023)	Rabbit	n/a	1;1,000
Cleaved Caspase-3 (Asp175)	Cell Signaling	(#9661)	Rabbit	n/a	1;1,000
Synaptopodin	American Research Products	#03-65194	Mouse	1:200	n/a
WT1	Santa Cruz Biotechnology	sc-192	Rabbit	1:100	n/a

Immunofluorescence and confocal microscopy in cell lines and tissue sections

Immunostaining was performed as described previously in immortalized human podocytes cell lines. Overexpression experiments were performed 24–48 hrs after transfection with Lipofectamine2000®. Immunostaining followed a standard protocol using permeabilization with 0.1% SDS for cells and 0.025 %Triton-X100 for paraffin embedded tissue sections (rat kidney, day 1 *postpartum).* Confocal imaging was performed using Leica SP5X system with an upright DM6000 microscope and images were processed with the Leica AF software suite. For lamellipodia staining (Figure 4) cells were grown at 37°C (non-permissive temperature) for 7 days, and were stimulated with recombinant Epidermal Growth Factor (EGF, Thermo Fisher) at a concentration of 100 ng/ml 20 min before staining. Immunofluorescence experiments were performed at least twice independently. Representative images are shown.

RNAi knockdown in human podocyte cell lines

pSirenRetroQ with shRNA against human *OSGEP, TP53RK,* and *TPRKB* was used for retroviral transduction of immortalized human podocyte cell lines (Dr. Moin Saleem, Bristol,

UK). Puromycin selected transduced cells. Due to growth defects, knockdown cells deteriorated after passage 4–5 (typically 12–14 days after transduction). Knockdown efficiency was confirmed for all experiments (Supplementary Fig. 24). For rescue experiments knockdown podocytes underwent a second lentiviral transduction with mouse mutant or wildtype cDNA of *Osgep, Tp53rk,* or *Tprkb*, respectively. (Expression control: Supplementary Fig. 26).

shRNA targets

Gene		shRNA target sequence
OSGEP (NM_017807.3)	shRNA# 1	GGTGTAATGTGAGGCTACAGGAGAT
	shRNA# 2	GGATTAACCTCCCAGGATATC
TP53RK (NM_033550.3)	shRNA# 3	GCTGAACATTGTGCTCATAGA
	shRNA# 5	GCTGAGTTTCATTTCAGCACT
TPRKB (NM_016058.2)	shRNA# 1	GCTGGACCTATTTCCCGAATG
	shRNA# 2	GCAGTTCACCTCTACAAACTG

Podocyte proliferation assay

The proliferation assay was performed using the xCELLigence system^{TM} with E-plates 16 (Roche Applied Science) according to the manufacturer's instructions. Experiments were performed 7 days after retroviral knockdown and 48 hrs after rescue transduction (if applicable), passage 4. For each condition, 2.5 x 10^4 cells were seeded in each well of the E-plate 16. Changes in impedance were analyzed using the RTCA software. Results were plotted as cell index (relative podocyte proliferation) vs. time. Each experiment was performed in triplicates, and repeated at least two times independently. Results are presented as mean ± standard deviation.

Colorimetric proliferation assay (BrdU incorporation)

Proliferation rate was assessed using a colorimetric BrdU assay kit (#6813, Cell signaling) according to the manufacturer's instructions. Experiments were performed in human immortalized podocytes 7 days after retroviral shRNA knockdown of *OSGEP, TP53RK*, or *TRPKB* (passage 4). BrdU incorporation is measured as absorbance at 450 nm using a spectrophotometer. Data is plotted as mean and standard deviation. Statistical significance was calculated using one-way ANOVA multi-test analysis with post hoc testing according to Sidak. P values <0.01 and <0.05 were considered statistically significant and are indicated in the figures. Measurements were performed in triplicates, and experiments were repeated twice independently.

Apoptosis assay and treatment with Mitomycin-C

Apoptosis in human podocyte cell lines with stable knockdown of *OSGEP, TP53RK,* and *TPRKB* was assessed using a colorimetric Caspase 3 Assay Kit (abcam, ab39401) following the manufacturer's instructions. Caspase-3 activity is measured as absorbance at 405 nm using a spectrophotometer. Data is plotted as mean and standard deviation. Statistical significance was calculated using one-way ANOVA multi-test analysis with post hoc testing

according to Sidak. P values <0.01 and <0.05 were considered statistically significant and are indicated in the figures. Individual measurements were performed in duplicates, and experiments were repeated three times independently. For Mitomycin-C (MMC) experiments, knockdown and control cells were treated with MMC (2.5 μg/ml) 12 hours prior to the experiment.

Podocyte migration assay

The migration rate of human podocyte cell lines with retroviral shRNA mediated knockdown of *OSGEP, TP53RK,* and *TPRKB* (5 days after knockdown, passage 3) was examined using the IncuCyte™ video-microscopy system (Essen Biosciences). For this assay, cells were seeded on a 96 well plate, grown to confluency, and a standardized scratch wound was made using the Woundmaker™ device as per protocol. Using live cell imaging wound closure was recorded in an hourly interval until the wound was fully closed. Subsequent data analysis was performed using the IncuCyte™ 96-well Kinetic Cell Migration and Invasion Assay software module. Individual data points are presented as mean ± standard deviation resulting from at least triplicate measurements. Experiments were repeated three times independently.

Telomeric Restriction Fragment

Measurement of the length of the terminal restriction fragments was performed by Southern blotting as previously described.[17]

Statistical analysis

Statistical analysis was performed using Graph Pad Prism®. Significances were calculated using unpaired one-way ANOVA with multiple comparisons and a standard confidence interval of 95%. Post hoc analysis was performed according to Sidak. P values <0.01 and <0.05 were considered statistically significant and are indicated in the figures.

Densitometry analysis of immunoblots

Densitometry analysis was performed using ImageJ.

REFERENCES for Online Methods

1. Chaki M, et al. Exome capture reveals ZNF423 and CEP164 mutations, linking renal ciliopathies to DNA damage response signaling. Cell. 2012; 150:533–48. [PubMed: 22863007]
2. Li H, et al. The Sequence Alignment/Map format and SAMtools. Bioinformatics. 2009; 25:2078–9. [PubMed: 19505943]
3. Seelow D, Schuelke M, Hildebrandt F, Nurnberg P. HomozygosityMapper--an interactive approach to homozygosity mapping. Nucleic Acids Res. 2009; 37:W593–9. [PubMed: 19465395]
4. Hildebrandt F, et al. A Systematic Approach to Mapping Recessive Disease Genes in Individuals from Outbred Populations. PloS Genetics. 2009; 5:31000353.
5. MacArthur DG, et al. Guidelines for investigating causality of sequence variants in human disease. Nature. 2014; 508:469–76. [PubMed: 24759409]
6. Halbritter J, et al. High-throughput mutation analysis in patients with a nephronophthisis-associated ciliopathy applying multiplexed barcoded array-based PCR amplification and next-generation sequencing. Journal of Medical Genetics. 2012; 49:756–767. [PubMed: 23188109]

7. Halbritter J, et al. Identification of 99 novel mutations in a worldwide cohort of 1,056 patients with a nephronophthisis-related ciliopathy. Hum Genet. 2013; 132:865–84. [PubMed: 23559409]
8. Montague TG, Cruz JM, Gagnon JA, Church GM, Valen E. CHOPCHOP: a CRISPR/Cas9 and TALEN web tool for genome editing. Nucleic Acids Res. 2014; 42:W401–7. [PubMed: 24861617]
9. Gagnon JA, et al. Efficient mutagenesis by Cas9 protein-mediated oligonucleotide insertion and large-scale assessment of single-guide RNAs. PLoS One. 2014; 9:e98186. [PubMed: 24873830]
10. Fu Y, Sander JD, Reyon D, Cascio VM, Joung JK. Improving CRISPR-Cas nuclease specificity using truncated guide RNAs. Nat Biotechnol. 2014; 32:279–84. [PubMed: 24463574]
11. Meeker ND, Hutchinson SA, Ho L, Trede NS. Method for isolation of PCR-ready genomic DNA from zebrafish tissues. Biotechniques. 2007; 43:610, 612, 614. [PubMed: 18072590]
12. Vouillot L, Thelie A, Pollet N. Comparison of T7E1 and surveyor mismatch cleavage assays to detect mutations triggered by engineered nucleases. G3 (Bethesda). 2015; 5:407–15. [PubMed: 25566793]
13. Kelley LA, Mezulis S, Yates CM, Wass MN, Sternberg MJ. The Phyre2 web portal for protein modeling, prediction and analysis. Nat Protoc. 2015; 10:845–58. [PubMed: 25950237]
14. Lipecka J, et al. Sensitivity of mass spectrometry analysis depends on the shape of the filtration unit used for filter aided sample preparation (FASP). Proteomics. 2016; 16:1852–7. [PubMed: 27219663]
15. Cox J, Mann M. MaxQuant enables high peptide identification rates, individualized p.p.b.-range mass accuracies and proteome-wide protein quantification. Nat Biotechnol. 2008; 26:1367–72. [PubMed: 19029910]
16. Tyanova S, et al. The Perseus computational platform for comprehensive analysis of (prote)omics data. Nat Methods. 2016; 13:731–40. [PubMed: 27348712]
17. Touzot F, et al. Function of Apollo (SNM1B) at telomere highlighted by a splice variant identified in a patient with Hoyeraal-Hreidarsson syndrome. Proc Natl Acad Sci U S A. 2010; 107:10097–102. [PubMed: 20479256]

Supplementary Material

Refer to Web version on PubMed Central for supplementary material.

Authors

Daniela A. Braun[1,*], Jia Rao[1,*], Geraldine Mollet[2,3,*], David Schapiro[1], Marie-Claire Daugeron[4], Weizhen Tan[1], Olivier Gribouval[2,3], Olivia Boyer[2,3,5], Patrick Revy[3,6], Tilman Jobst-Schwan[1], Johanna Magdalena Schmidt[1], Jennifer A. Lawson[1], Denny Schanze[7], Shazia Ashraf[1], Nathalie Boddaert[3,8,9], Bruno Collinet[4,10], Gaëlle Martin[2,3], Dominique Liger[4], Svjetlana Lovric[1], Monica Furlano[2,3,11], I. Chiara Guerrera[12], Oraly Sanchez-Ferras[13], Björn Menten[14], Sarah Vergult[14], Nina De Rocker[14], Merlin Airik[1], Tobias Hermle[1], Shirlee Shril[1], Eugen Widmeier[1,15], Heon Yung Gee[1,16], Won-Il Choi[1], Carolin E. Sadowski[1], Werner L. Pabst[1], Jillian Warejko[1], Ankana Daga[1], Tamara Basta LeBerre[4], Verena Matejas[17], Babak Behnam[18,19], Brendan Beeson[20], Amber Begtrup[21], Malcolm Bruce[20], Gaik-Siew Ch'ng[22], Shuan-Pei Lin[23,24], Jui-Hsing Chang[23], Chao-Huei Chen[25], Megan T. Cho[21], Patrick E. Gipson[26], Chyong-Hsin Hsu[23], Jameela A. Kari[27], Yu-Yuan Ke[25], Cathy Kiraly-Borri[28], Wai-ming Lai[29], Emmanuelle Lemyre[30], Rebecca Okasha Littlejohn[31], Amira Masri[32], Mastaneh Moghtaderi[33], Kazuyuki Nakamura[34], Marleen Praet[35], Chitra Prasad[36], Agnieszka Prytula[37], Elizabeth Roeder[38,39], Patrick Rump[40], Rhonda E. Schnur[21], Takashi Shiihara[41], Manish Sinha[42], Neveen A Soliman[43], Kenza Soulami[44], David A. Sweetser[45], Wen-Hui Tsai[46], Jeng-Daw Tsai[23,47], Udo Vester[48], David H. Viskochil[49], Nithiwat Vatanavicharn[50], Jessica L.

Waxler[45], Matthias T.F. Wolf[51], Sik-Nin Wong[52], Annapurna Poduri[53,54], Gessica Truglio[53], Shrikant Mane[55], Richard P. Lifton[55,56], Maxime Bouchard[13], Peter Kannu[57], David Chitayat[57], Daniella Magen[58], Bert Calleweart[14], Herman van Tilbeurgh[4], Martin Zenker[7], Corinne Antignac[2,3,59], and Friedhelm Hildebrandt[1]

Affiliations

[1]Department of Medicine, Boston Children's Hospital, Harvard Medical School, Boston, Massachusetts, USA [2]INSERM, U1163, Imagine Institute, Laboratory of Hereditary Kidney Diseases, Paris, France [3]Paris Descartes-Sorbonne Paris Cité University, Paris, France [4]CNRS-CEA UMR9198, Université Paris-sud, Institut de Biologie Intégrative de la Cellule, Orsay, France [5]Department of Pediatric Nephrolology, Necker Hospital, Assistance Publique - Hôpitaux de Paris, Paris, France [6]INSERM, U1163, Imagine Institute, Laboratory of Genome dynamics in the Immune system, Paris, France [7]Institute of Human Genetics, University Hospital Magdeburg, Magdeburg, Germany [8]INSERM, U1163, Imagine Institute, Laboratory of Molecular and Pathophysiological Bases of Cognitive Disorders, Paris, France [9]Department of Pediatric Neuroradiology, Necker Hospital, Assistance Publique - Hôpitaux de Paris, Paris, France [10]Sorbonne Universités UPMC, UFR 927, Sciences de la vie, Paris, France [11]Nephrology Department, Fundació Puigvert, IIB Sant Pau, Universitat Autònoma de Barcelona and REDINREN, Barcelona, Spain [12]INSERM U1151 and Proteomics Platform Necker, SFR Necker, Paris Descartes-Sorbonne Paris Cité University, Paris, France [13]Goodman Cancer Research Centre and Department of Biochemistry, McGill University, Montreal, Canada [14]Center for Medical Genetics, Ghent University Hospital, Ghent, Belgium [15]Department of Medicine, Renal Division, Medical Center-University of Freiburg, Faculty of Medicine, University of Freiburg, Germany [16]Department of Pharmacology, Brain Korea 21 PLUS Project for Medical Sciences, Yonsei University College of Medicine, Seoul, Republic of Korea [17]Institute of Human Genetics, Friedrich-Alexander-Universität Erlangen-Nürnberg, Erlangen, Germany [18]Department of Medical Genetics and Molecular Biology, Iran University of Medical Sciences (IUMS), Tehran, Iran [19]Medical Genetics Branch National Human Genome Research Institute & NIH Undiagnosed Diseases Program, Common Fund, Office of the Director, National Institutes of Health, Bethesda, Maryland, USA [20]Department of Diagnostic Imaging, Princess Margaret and King Edward Memorial Hospitals, Perth, Australia [21]GeneDx, Gaithersburg, MD, USA [22]Department of Genetics, Kuala Lumpur Hospital, Kuala Lumpur, Malaysia [23]Department of Pediatrics, MacKay Children's Hospital, Taipei, Taiwan [24]Department of Medicine, MacKay Medical College, New Taipei City, Taiwan [25]Department of Pediatrics, Taichung Veterans General Hospital, Taichung, Taiwan [26]Internal Medicine and Pediatrics Divisions of Adult and Pediatric Nephrology, University of Michigan, 3914 Taubman Center, SPC 5364, Ann Arbor, USA [27]Pediatric nephrology center of excellence and Pediatric Department, King Abdulaziz University, Jeddah, Saudi Arabia [28]Genetic Services of Western Australia, Princess Margaret Hospital for Children and King Edward Memorial Hospital for Women, Subiaco, 6008, WA, Australia [29]Department of Paediatrics & Adolescent Medicine, Princess Margaret Hospital, 2-10 Princess

Margaret Hospital Road, Hong Kong, China [30]Service de génétique médicale, département de Pédiatrie, CHU Sainte-Justine, Université de Montréal, Montréal, Québec, Canada [31]Department of Pediatrics, Baylor College of Medicine, San Antonio, Texas, USA [32]Department of Pediatrics, Division of Child Neurology, Faculty of Medicine, The University of Jordan, Jordan [33]Golestan University of Medical Sciences, Gorgan, Iran [34]Department of Biochemistry and Functional Proteomics, Yamaguchi University Graduate School of Medicine, Ube, Yamaguchi, Japan [35]Department of Pathology, Ghent University Hospital, Ghent, Belgium [36]Department of Genetics, Metabolism and Pediatrics; Western University, London Health Sciences Centre, London, ON Canada [37]Department of Pediatrics, Ghent University Hospital, Ghent, Belgium [38]Department of Pediatrics, Baylor College of Medicine, San Antonio, Texas, USA [39]Department of Molecular and Human Genetics, Baylor College of Medicine, San Antonio, Texas, USA [40]University of Groningen, University Medical Center Groningen, Department of Genetics, Netherlands [41]Department of Pediatrics, Yamagata University School of Medicine, 2-2-2 Iida-nishi, Yamagata 990-9585, Japan [42]Kings College London Department of Paediatric Nephrology, Evelina London Children's Hospital, Guys and St Thomas's NHS FoundationTrust, London, United Kingdom [43]Department of Pediatrics, Center of Pediatric Nephrology & Transplantation, Cairo University, Egyptian Group for Orphan Renal Diseases, Cairo, Egypt [44]Department of Nephrology, Ibn Rochd University Hospital, Casablanca, Morocco [45]Division of Medical Genetics, Massachusetts General Hospital for Children, Boston, Massachusetts [46]Division of Genetics and Metabolism, Department of Pediatrics, Chi Mei Medical Center, Tainan 710, Taiwan [47]Department of Pediatrics, Taipei Medical University, Taipei, Taiwan [48]Department of Pediatrics II, University Hospital Essen, Essen, Germany [49]Departments of Pediatrics, Division of Medical Genetics, University of Utah, School of Medicine, Salt Lake City, Utah, USA [50]Division of Medical Genetics, Department of Pediatrics, Faculty of Medicine Siriraj Hospital, Mahidol University, Bangkok, Thailand [51]Division of Pediatric Nephrology, Department of Pediatrics, University of Texas Southwestern Medical Center, Dallas, Texas 75390-9063, USA [52]Department of Pediatrics & Adolescent Medicine, Tuen Mun Hospital, Tsing Chung Koon Road, Tuen Mun, Hong Kong, China [53]Epilepsy Genetics Program and F.M. Kirby Neurobiology Center, Department of Neurology, Boston Children's Hospital, Boston, Massachusetts, USA [54]Department of Neurology, Harvard Medical School, Boston, Massachusetts, USA [55]Department of Genetics, Yale University School of Medicine, New Haven, CT 06510, USA [56]Howard Hughes Medical Institute, Chevy Chase, Maryland 20815, USA [57]Department of Pediatrics, Division of Clinical and Metabolic Genetics, The Hospital for Sick Children, Toronto, ON, Canada [58]Pediatric Nephrology Institute, Rambam Health Care Campus, Haifa, Israel [59]Department of Genetics, Necker Hospital, Assistance Publique - Hôpitaux de Paris, Paris, France

Acknowledgments

We are grateful to the families and study individuals for their contribution.

We thank the Yale Center for Mendelian Genomics (U54HG006504) and the Care4Rare Canada Consortium for whole exome sequencing.

We acknowledge Dr. Daisuke Ogino, pediatric nephrologist, Yamagata University, for providing the nephrology data regarding patient B60, Dr. Hervé Sartelet, Département de Pathologie, CHU-Sainte-Justine, Université de Montréal, for providing pathology pictures from the renal biopsy from patient B80, and Dr. Sonbol Ameli, Children's Medical Center, Tehran University of Medical Sciences, for providing DNA samples of family B50.

We thank Prof. Dr. André Reis and Dr. Arif Ekici, Institute of Human Genetics, University of Erlangen-Nuremberg, for supporting the initial Galloway-Mowat syndrome mapping study conducted by M.Z.

This research was supported by grants from the National Institutes of Health to F.H. (DK076683) and by the Howard Hughes Medical Institute to F.H.

F.H. is the Warren E. Grupe Professor.

W.T. is supported by the ASN Foundation for Kidney Research.

Ba.B. is supported in part by the Intramural Research Program of the National Human Genome Research Institute, National Institutes of Health, Bethesda, Maryland, USA (Common Fund).

N.dR., S.V., and B.C. are a research fellow, a postdoctoral research fellow, and a senior clinical investigator of the Fund for Scientific Research, Flanders, respectively.

E.W. is supported by the German National Academy of Sciences Leopoldina (LPDS-2015-07).

H.Y.G. is supported by the National Research Foundation of Korea, Ministry of Science, ICT and Future planning (2015R1D1A1A01056685) and faculty seed money from the Yonsei University College of Medicine (2015-32-0047).

M.T.F.W. is supported by K08-DK095994-05 (NIH) and Children's Clinical Research Advisory Committee (CCRAC), Children's Medical Center, Dallas.

M.B. holds a Senior Research Scholar Award from Fonds de la Recherche du Québec-Santé (FRQS) and is supported by a grant from the Canadian Institutes for Health Research (MOP-84470).

O.S.F. is supported by the KRESCENT Post-Doctoral Fellowship and the MicGill Integrated Cancer Research Training (MICRTP) fellowship.

T.J.S. is supported by the grant Jo 1324/1-1 of the Deutsche Forschungsgemeinschaft (DFG).

C.A was supported by grants from the Agence Nationale de la Recherche (GenPod project ANR-12-BSV1-0033.01), the European Union’s Seventh Framework Programme (FP7/2007-2013/no 305608-EURenOmics), the Fondation Recherche Médicale (DEQ20150331682) and the ‘‘Investments for the Future’’ program (ANR-10-IAHU-01).

M.F. was supported by grants from the Spanish Society of Nephrology and the Catalan Society of Nephrology.

M.D.S. acknowledges financial support from the Department of Health by the National Institute for Health Research (NIHR) comprehensive Biomedical Research Centre award to Guy's & St Thomas' NHS Foundation Trust in partnership with King's College London and King's College Hospital NHS Foundation Trust.

M.Z. was supported by the Deutsche Forschungsgemeinschaft (SFB423).

References

1. Vodopiutz J, et al. WDR73 Mutations Cause Infantile Neurodegeneration and Variable Glomerular Kidney Disease. Hum Mutat. 2015; 36:1021–8. [PubMed: 26123727]

2. Jinks RN, et al. Recessive nephrocerebellar syndrome on the Galloway-Mowat syndrome spectrum is caused by homozygous protein-truncating mutations of WDR73. Brain. 2015; 138:2173–90. [PubMed: 26070982]
3. Colin E, et al. Loss-of-function mutations in WDR73 are responsible for microcephaly and steroid-resistant nephrotic syndrome: Galloway-Mowat syndrome. Am J Hum Genet. 2014; 95:637–48. [PubMed: 25466283]
4. Hildebrandt F, et al. A Systematic Approach to Mapping Recessive Disease Genes in Individuals from Outbred Populations. PloS Genetics. 2009; 5:31000353.
5. Chaki M, et al. Exome Capture Reveals ZNF423 and CEP164 Mutations, Linking Renal Ciliopathies to DNA Damage Response Signaling. Cell. 2012; 150:533–548. [PubMed: 22863007]
6. Daugeron MC, et al. Gcn4 misregulation reveals a direct role for the evolutionary conserved EKC/KEOPS in the t6A modification of tRNAs. Nucleic Acids Res. 2011; 39:6148–60. [PubMed: 21459853]
7. El Yacoubi B, et al. A role for the universal Kae1/Qri7/YgjD (COG0533) family in tRNA modification. EMBO J. 2011; 30:882–93. [PubMed: 21285948]
8. Srinivasan M, et al. The highly conserved KEOPS/EKC complex is essential for a universal tRNA modification, t6A. EMBO J. 2011; 30:873–81. [PubMed: 21183954]
9. Yarian C, et al. Accurate translation of the genetic code depends on tRNA modified nucleosides. J Biol Chem. 2002; 277:16391–5. [PubMed: 11861649]
10. Downey M, et al. A genome-wide screen identifies the evolutionarily conserved KEOPS complex as a telomere regulator. Cell. 2006; 124:1155–68. [PubMed: 16564010]
11. Oberto J, et al. Qri7/OSGEPL, the mitochondrial version of the universal Kae1/YgjD protein, is essential for mitochondrial genome maintenance. Nucleic Acids Res. 2009; 37:5343–52. [PubMed: 19578062]
12. Kisseleva-Romanova E, et al. Yeast homolog of a cancer-testis antigen defines a new transcription complex. EMBO J. 2006; 25:3576–85. [PubMed: 16874308]
13. Hecker A, et al. The universal Kae1 protein and the associated Bud32 kinase (PRPK), a mysterious protein couple probably essential for genome maintenance in Archaea and Eukarya. Biochem Soc Trans. 2009; 37:29–35. [PubMed: 19143597]
14. Peterson D, et al. A chemosensitization screen identifies TP53RK, a kinase that restrains apoptosis after mitotic stress. Cancer Res. 2010; 70:6325–35. [PubMed: 20647325]
15. Sadowski CE, et al. A Single-Gene Cause in 29.5% of Cases of Steroid-Resistant Nephrotic Syndrome. J Am Soc Nephrol. 2014; 26:1279–89. [PubMed: 25349199]
16. Halbritter J, et al. Identification of 99 novel mutations in a worldwide cohort of 1,056 patients with a nephronophthisis-related ciliopathy. Hum Genet. 2013; 132:865–84. [PubMed: 23559409]
17. Hildebrandt F, Heeringa SF. Specific podocin mutations determine age of onset of nephrotic syndrome all the way into adult life. Kidney Int. 2009; 75:669–71. [PubMed: 19282856]
18. Ruf RG, et al. Patients with mutations in NPHS2 (podocin) do not respond to standard steroid treatment of nephrotic syndrome. J Am Soc Nephrol. 2004; 15:722–32. [PubMed: 14978175]
19. Mao DY, et al. Atomic structure of the KEOPS complex: an ancient protein kinase-containing molecular machine. Mol Cell. 2008; 32:259–75. [PubMed: 18951093]
20. Hecker A, et al. Structure of the archaeal Kae1/Bud32 fusion protein MJ1130: a model for the eukaryotic EKC/KEOPS subcomplex. EMBO J. 2008; 27:2340–51. [PubMed: 19172740]
21. Zhang W, et al. Crystal structures of the Gon7/Pcc1 and Bud32/Cgi121 complexes provide a model for the complete yeast KEOPS complex. Nucleic Acids Res. 2015; 43:3358–72. [PubMed: 25735745]
22. O'Driscoll M, Jeggo PA. The role of the DNA damage response pathways in brain development and microcephaly: insight from human disorders. DNA Repair (Amst). 2008; 7:1039–50. [PubMed: 18458003]
23. Griffith E, et al. Mutations in pericentrin cause Seckel syndrome with defective ATR-dependent DNA damage signaling. Nat Genet. 2008; 40:232–6. [PubMed: 18157127]
24. Ameziane N, et al. A novel Fanconi anaemia subtype associated with a dominant-negative mutation in RAD51. Nat Commun. 2015; 6:8829. [PubMed: 26681308]

25. O'Driscoll M, Ruiz-Perez VL, Woods CG, Jeggo PA, Goodship JA. A splicing mutation affecting expression of ataxia-telangiectasia and Rad3-related protein (ATR) results in Seckel syndrome. Nat Genet. 2003; 33:497–501. [PubMed: 12640452]
26. Wharram BL, et al. Podocyte depletion causes glomerulosclerosis: diphtheria toxin-induced podocyte depletion in rats expressing human diphtheria toxin receptor transgene. J Am Soc Nephrol. 2005; 16:2941–52. [PubMed: 16107576]
27. Costessi A, et al. The human EKC/KEOPS complex is recruited to Cullin2 ubiquitin ligases by the human tumour antigen PRAME. PLoS One. 2012; 7:e42822. [PubMed: 22912744]
28. Walne AJ, Vulliamy T, Kirwan M, Plagnol V, Dokal I. Constitutional mutations in RTEL1 cause severe dyskeratosis congenita. Am J Hum Genet. 2013; 92:448–53. [PubMed: 23453664]
29. Kristensen AR, Gsponer J, Foster LJ. A high-throughput approach for measuring temporal changes in the interactome. Nat Methods. 2012; 9:907–9. [PubMed: 22863883]
30. Suraneni P, et al. The Arp2/3 complex is required for lamellipodia extension and directional fibroblast cell migration. J Cell Biol. 2012; 197:239–51. [PubMed: 22492726]
31. Faul C, Asanuma K, Yanagida-Asanuma E, Kim K, Mundel P. Actin up: regulation of podocyte structure and function by components of the actin cytoskeleton. Trends Cell Biol. 2007; 17:428–37. [PubMed: 17804239]
32. Gee HY, et al. ARHGDIA mutations cause nephrotic syndrome via defective RHO GTPase signaling. J Clin Invest. 2013; 123:3243–53. [PubMed: 23867502]
33. Gee HY, et al. KANK deficiency leads to podocyte dysfunction and nephrotic syndrome. J Clin Invest. 2015; 125:2375–84. [PubMed: 25961457]
34. Ashraf S, et al. ADCK4 mutations promote steroid-resistant nephrotic syndrome through CoQ10 biosynthesis disruption. J Clin Invest. 2013; 123:5179–89. [PubMed: 24270420]

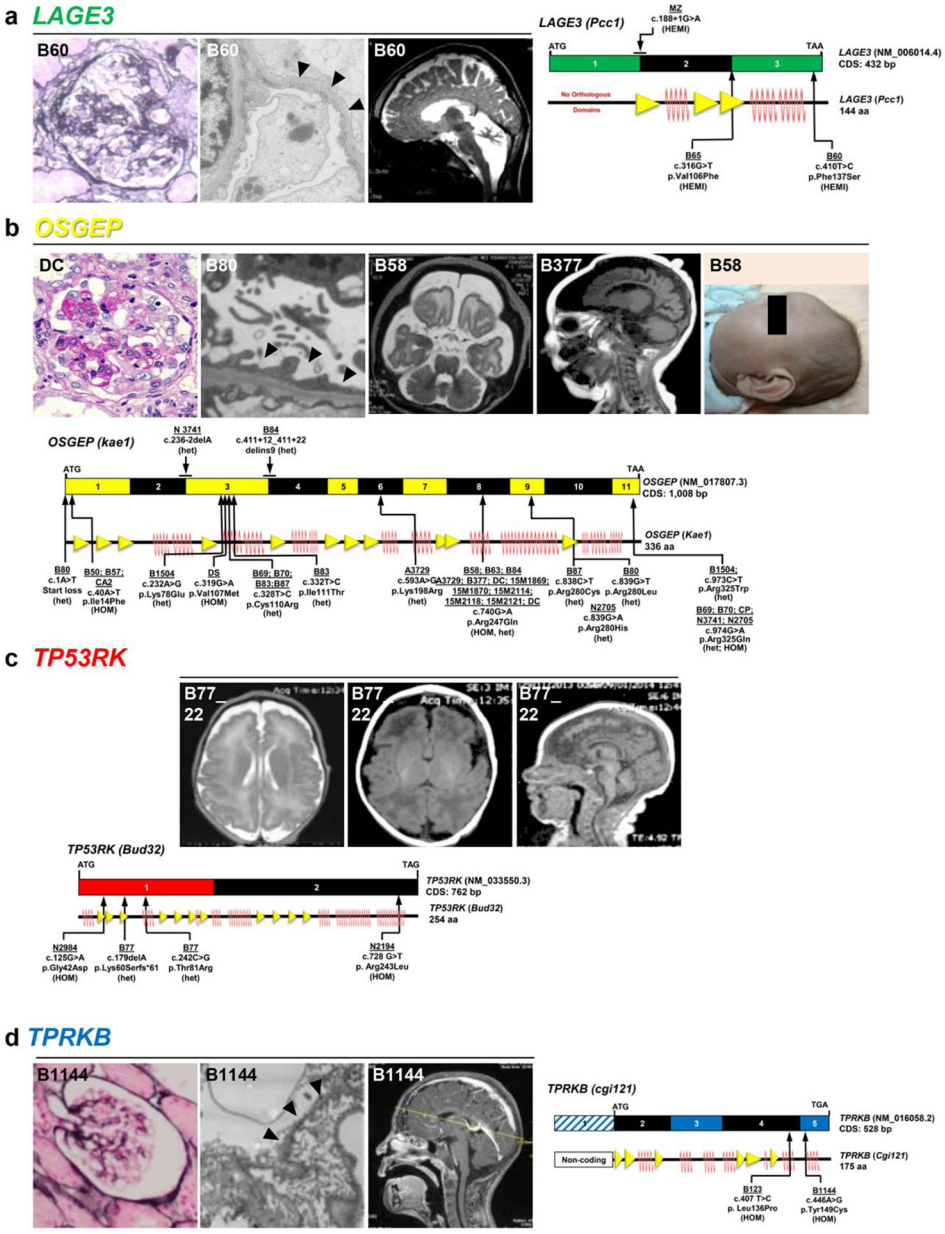

Figure 1. Whole exome sequencing identifies recessive mutations in the 4 KEOPS complex encoding genes *LAGE3, OSGEP, TP53RK, TPRKB* in 30 families with GAMOS 2–5

(a–d) Left or upper panels show clinical phenotype of individuals with recessive mutations, right or lower panels show exon structures and secondary structures of human *LAGE3* (a), *OSGEP* (b), *TP53RK* (c), and *TPRKB* (d) cDNA. Positions of start codons and of stop codons are indicated. Predicted secondary structure is indicated for beta strand and α-helix conformation as triangle and zigzag lines, respectively.

(a) Clinical features of individual B60 with a hemizygous mutation of *LAGE3*: Renal histology showing FSGS, transmission electron microscopy (TEM) showing podocyte foot process effacement (arrowheads), and MRI showing microcephaly with polymicrogyria and diffuse cerebellar atrophy.

(b) Clinical features of individuals 'DC', B80, B58, and B377 with mutations of *OSGEP*: Renal histology of individual 'DC' showing FSGS, and TEM of B80 showing foot process effacement (arrow heads). Cranial imagining of individuals B58 and B377 showing microcephaly, reduced gyration, and diffuse cortical atrophy. Clinical photograph of B58 showing severe deformation of the forehead.

(c) Clinical features of individual B77_22 with compound heterozygous mutations of *TP53RK*: Cranial imaging showing microcephaly and polymicrogyria.

(d) Clinical features of individual B1144 with a homozygous mutation of *TPRKB*: Renal histology showing FSGS and TEM showing podocyte foot process effacement (arrow heads). Brain MRI showing microcephaly and pachygyria. HEMI, hemizygous; het, heterozygous; HOM, homozygous.

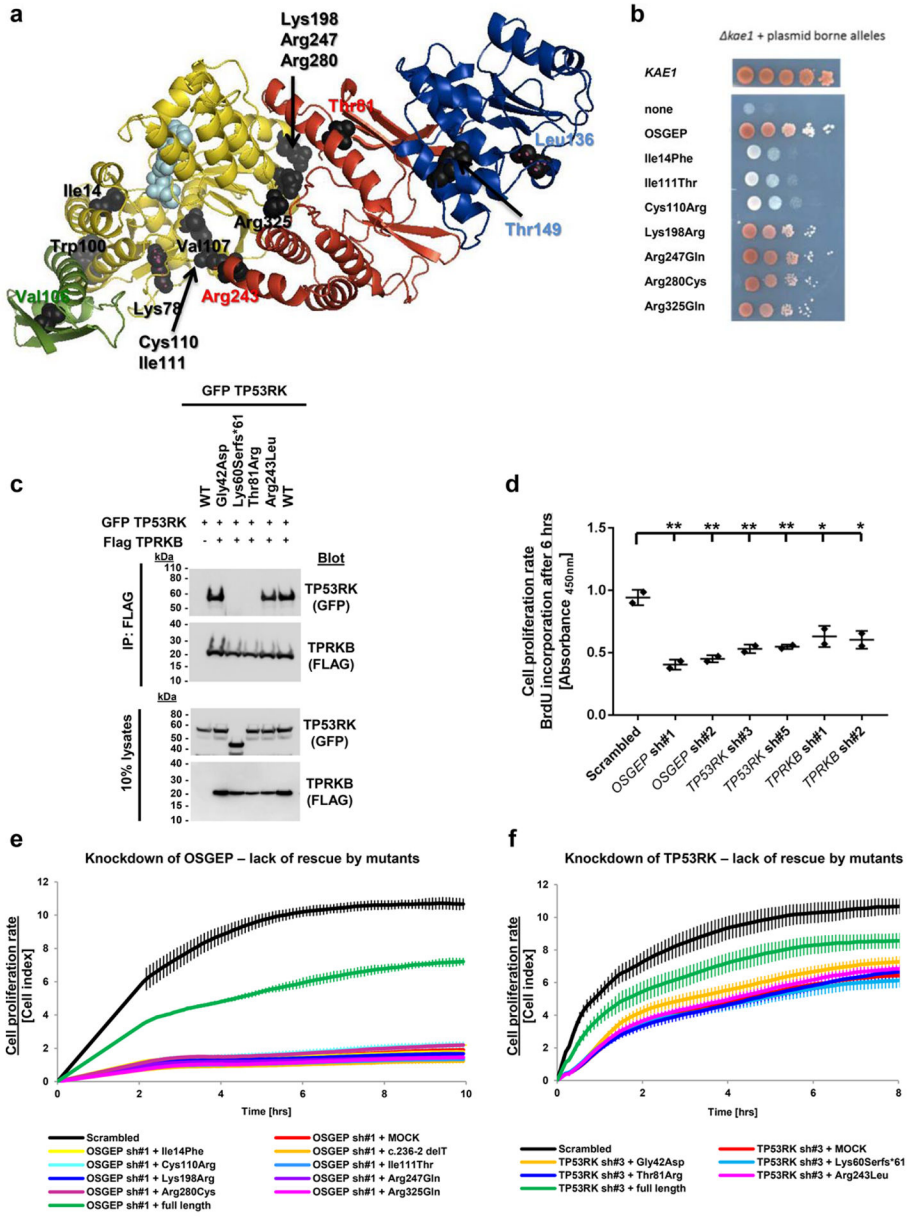

Figure 2. *TP53RK* mutations abrogate interaction with TPRKB, and GAMOS mutations fail to rescue cell proliferation rate decreased by knockdown of *OSGEP* or *TP53RK*

(a) Structural modeling of KEOPS mutations. The three-dimensional representation of the human KEOPS complex is based on structural information of subcomplexes from archeae and yeast. Subunits are represented in different colors: LAGE3 (green), OSGEP (yellow), TP53RK (red) and TPRKB (blue). The residues corresponding to missense mutations identified in patients with GAMOS2–5 are mapped as black spheres and their corresponding positions are written in green (LAGE3), black (OSGEP), red (TPR53K) and blue (TPRKB). A model of a nucleotide bound in the active site of OSGEP is represented as cyan spheres.

(b) Overexpression of human OSGEP in a Δkae1 (orthologous yeast gene) yeast strain partially rescues the Δkae1 associated growth defect. Each horizontal panel corresponds to

tenfold serial dilution of the cell suspension. The extent of growth complementation was assessed by comparison with full complementation (KAE1) and no complementation (none). Overexpressed alleles are indicated on the left. Mutants OSGEP alleles fall into two classes: hypomorphic alleles (Lys198Arg, Arg247Gln, Arg280Cys, Arg325Gln) and amorphic alleles (Ile14Phe, Ile111Thr, Cys110Arg).

(c) Co-immunoprecipitation of FLAG-tagged full-length wildtype ***TPRKB*** with GFP-tagged wildtype ***TP53RK*** or mutant ***TP53RK*** cDNA constructs that reflect the GAMOS mutations. Constructs reflecting the TP53RK mutants p.Lys60Serfs*61 and p.Thr81Arg abrogate interaction with TPRKB.

(d) A colorimetric BrdU assay demonstrates that human podocytes with stable knockdown of ***OSGEP, TP53RK, and TPRKB*** exhibit reduced cell proliferation rates. Cells are at passage 3 after transduction, * indicates $p<0.05$, **indicates $p<0.01$ calculated by one-way ANOVA.

(e–f) Proliferation rate of human immortalized podocytes was assayed using the xCELLigence® system. Cells are at passage 4 after stable transduction with shRNA targeting ***OSGEP*** and ***TP53RK.***

(e) ***OSGEP*** knockdown reduced podocyte proliferation rate (red), which was rescued by stable overexpression of mouse wildtype, full-length ***Osgep*** (green), but not of mutant constructs reflecting the mutations identified in individuals with GAMOS.

(f) ***TP53RK*** knockdown reduced podocyte proliferation rate (red), which was rescued by stable overexpression of mouse wildtype, full-length ***Tp53rk*** (green), but not of mutant ***Tp53rk*** constructs reflecting the mutations identified in individuals with GAMOS.

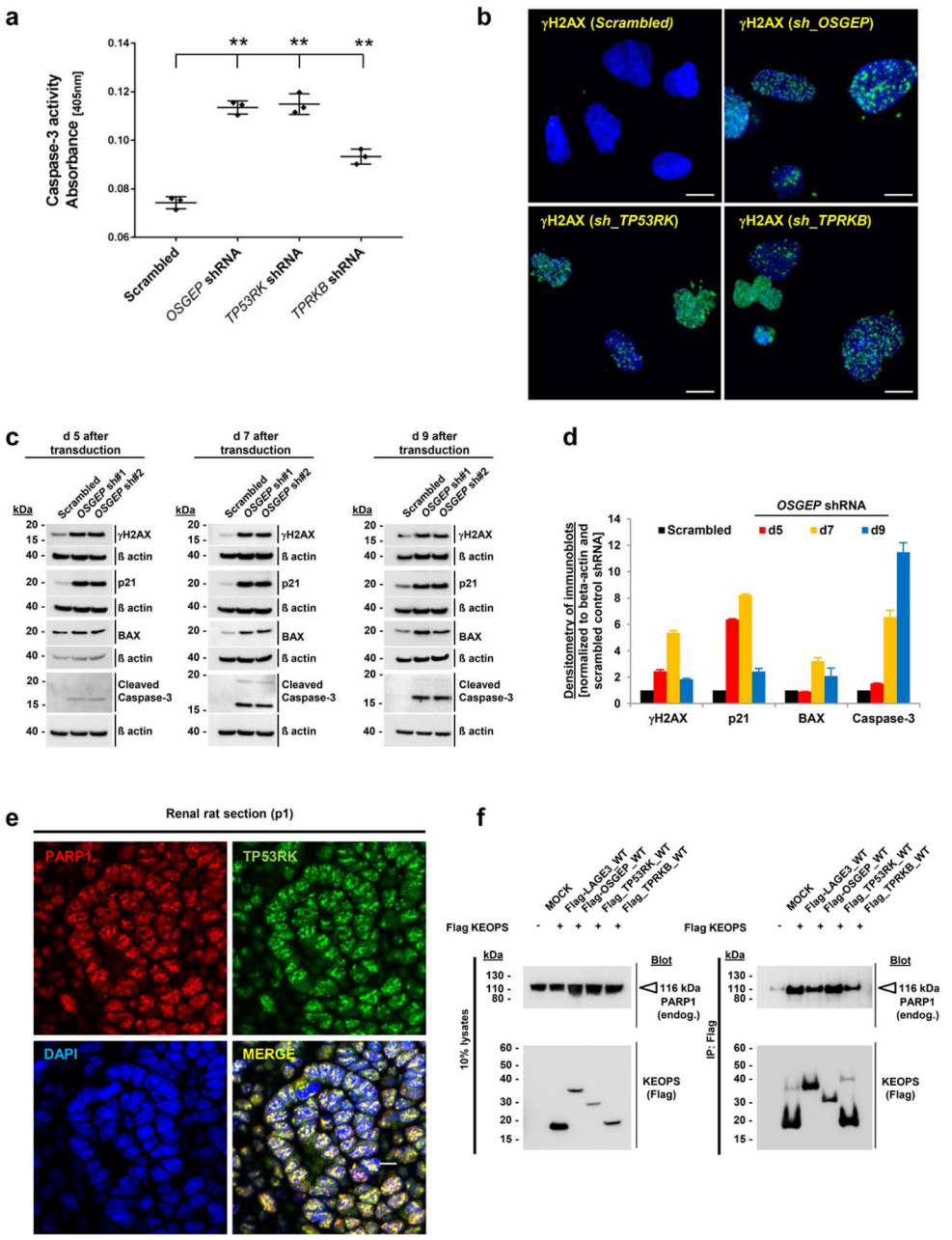

Figure 3. Knockdown of *OSGEP*, *TP53RK*, or *TPRKB* in human podocytes induces DNA damage response signaling (DDR) and subsequently apoptosis

(a) In a colorimetric assay, knockdown of ***OSGEP***, ***TP53RK,*** or ***TPRKB*** in human podocytes increases caspase-3 activity indicating apoptotic cell death. Cells are at passage 4 after transduction, **indicates $p<0.01$ calculated by one-way ANOVA.

(b) Staining with an antibody against phosphorylated histone H2A.X (γH2AX) was increased in human podocytes 7 days after stable shRNA knockdown of ***OSGEP***, ***TP53RK,*** or ***TPRKB*** (passage 3) as compared to scrambled control cells indicating induction of DDR. DAPI stains DNA (blue). Scale bar 10μm. Quantification of 100 cells for each condition is shown in Suppl. Fig. 16A.

(c) Compared to scrambled shRNA transfected control cells, knockdown of ***OSGEP*** in human podocytes increases γH2AX and CDK inhibitor p21 on days 5, 7, and 9 after knockdown. Strong increase of the proapoptotic factor BAX and cleaved caspase-3 is only observed on days 7 and 9.

(d) Densitometry of the intensity of immunoblot signals of γH2AX, p21, BAX, and cleaved caspase-3 in human immortalized podocytes cell lines was measured using ImageJ. Absolute values were normalized to beta actin (loading controls). Intensities of scrambled control cells (black) were normalized as 1. Data points are presented as mean of two OSGEP shRNAs and standard deviation. Knockdown of ***OSGEP*** results in an increase of γH2AX and p21 on days 5,7, and 9 after knockdown. In contrast, BAX and cleaved caspase-3 only show strong induction on days 7 and 9 after transduction demonstrating that the activation of DDR (γH2AX) precedes the induction of apoptosis (BAX, cleavage of caspase-3) upon knockdown of ***OSGEP***. The decrease of signals for γH2AX, p21, and BAX on day 9 is likely explained by apoptotic cell death.

(f) Staining of renal rat sections (p1) with antibodies against PARP1 and TP53RK demonstrates that both proteins colocalize to PARP1 positive nuclear foci in renal glomeruli. DAPI stains DNA (blue). Scale bars are 7.5 μm.

(g) Upon overexpression Flag-tagged LAGE3, OSGEP, TP53RK, and TPRKB immunoprecipitate endogenous PARP1 in HEK293T cells.

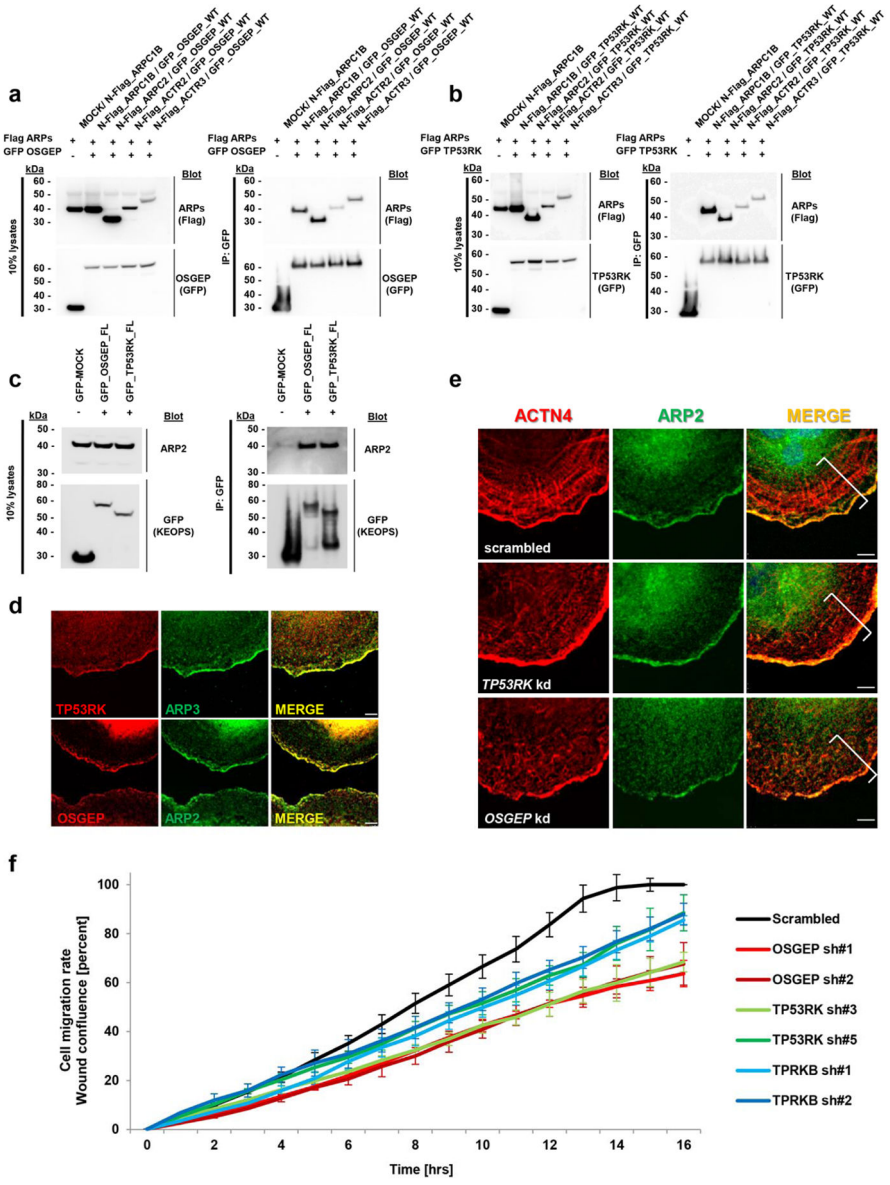

Figure 4. OSGEP and TP53RK colocalize with the ARP2/3 complex at lamellipodia of podocytes, and knockdown disrupts the actin cytoskeleton and impairs cell migration

(a–b) Upon co-overexpression in HEK293T cells GFP-tagged OSGEP **(a)** and TP53RK **(b)** interact with 4 FLAG-tagged proteins of the ARP2/3 complex, namely ARPC1B, ARPC2, ACTR2, and ACTR3.

(c) Half-endogenous co-immunoprecipitation of GFP-tagged OSGEP and TP53RK confirms interaction with endogenous ARP2 in HEK293T cells.

(d) Upon EGF stimulation (100 ng/ml, 20 min) to induce lamellipodia formation, OSGEP (red) and TP53RK (red) co-localize with ARP2 (green) and ARP3 (green) at lamellipodia of differentiated human podocytes. The panels show a 100 x magnification of lamellipodia. Scale bars are 7.5 μm.

(e) Upon EGF stimulation (100 ng/ml, 20 min) of differentiated podocytes, actin stress fibers (labelled red with α-ACTN4 antibody) radiate as actin fans to support the sub-lamellipodia network (white bracket). Note that in ***OSGEP*** and ***TP53RK*** knockdown cell lines the formation of the actin fan supporting lamellipodia is severely disrupted. Scale bars are 7.5 μm. Cells are at passage 3 after stable transduction with shRNA targeting ***OSGEP*** or ***TP53RK***, respectively.

(f) Cell migration rate of human immortalized podocytes was assessed using the IncuCyte™ system to measure wound closure as representing podocyte migration rate in real-time. 45,000 cells were seeded for each condition. Experiments are performed 5 days after stable transduction with shRNA against KEOPS genes (passage 3). Note that compared to control cells (black line), knockdown of ***OSGEP*** (red lines), ***TP53RK*** (green lines), and ***TPRKB*** (blue lines) with two different shRNAs for each gene reduced podocyte migration rate ***in vitro***.

TABLE 1

Phenotypic spectrum in 33 individuals of 30 families with mutations of *LAGE3, OSGEP, TP53RK,* and *TPRKB* and Galloway-Mowat syndrome (GAMOS 2–5)
(For additional information see Supplementary Table 1.)

		# of patients	Median age	Range
Gender	Male/female	20/13		
Ethnicity	Asian	15		
	Caucasian (Iran)	4		
	European American	5		
	Hispanic	2		
	Arabic	3		
	African	1		
	American Indian	1		
	Other	2		
Renal involvement	Proteinuria	33/33	3 mon (n=33)	At birth - 4.5 yrs
	Kidney Histology	17/33		
	FSGS NOS	9		
	Collapsing FSGS	1		
	DMS	2		
	MCNS	2		
	Foot process effacement NOS	2		
	Other	1		
	Not performed	16		
	ESKD	17/33	9 mon (n=16)	1 mon - 8 yrs
	No ESKD before death or no data	16/33		
Neurological involvement	Primary microcephaly	33/33		
	Hypotonia	15		
	Spasticity	9		
	Developmental delay	26		
	Seizures / abnormal EEG	17		
	Gyral defects	16		
	Myelination defects / white matter anomalies	16		
	Cortical atrophy	10		
	Cerebellar atrophy	10		
Facial dysmorphism	Progeroid (old appearing)	12		
	Ear anomalies (large, floppy or low set)	15		
	Micrognathia	14		
	Hypertelorism	8		
Skeletal features	Arachnodactyly / camptodactyly	15		
	Short stature	7		

		# of patients	Median age	Range
Other	Intrauterine growth retardation	9		
	Visual impairment	6		
	Hearing impairment	4		
	Heart involvement (ASD)	3		
Survival	Death before 3 years of age	24	6 mon (n= 26)	6 weeks-25 yrs (n=26)
	Alive at present	5		
	No data / death >3 yrs	4		

Notes: ASD, Atrial septal defect; DMS, diffuse mesangial sclerosis; EEG, electroencephalogram; ESKD, end stage kidney disease; FSGS, focal segmental glomerulosclerosis; NOS, Not Otherwise Specified; IUGR, intrauterine growth restriction; MCNS, minimal change nephrotic syndrome; mon, months; yrs., years.